Space Vector PWM Control of Dual Three-Phase Induction Machine Using Vector Space Decomposition

Yifan Zhao, *Student Member, IEEE*, and Thomas A. Lipo, *Fellow, IEEE*

Abstract— **The technique of vector space decomposition control of voltage source inverter fed dual three-phase induction machines is presented in this paper. By vector space decomposition, the analytical modeling and control of the machine are accomplished in three two-dimensional orthogonal subspaces and the dynamics of the electromechanical energy conversion related and the nonelectromechanical energy conversion related machine variables are thereby totally decoupled. A space vector PWM technique is also developed based on the vector space decomposition to limit the 5th, 7th, 17th, 19th, ... harmonic currents which in such a system would be otherwise difficult to control. The techniques developed in this paper can be generalized for the control of an induction machine with an arbitrary number of phases.**

I. Introduction

HIGH-POWER electric machine drive systems have found many applications such as pumps, fans, compressors, rolling mills, cement mills, mine hoists, just to name a few. At present, the most successful type of the high power drive systems are cycloconverter-electric machine drives and synchronous machines fed by current source thyristor inverters. Voltage source inverters, despite their advantage in line power factor over a cycloconverter as well as their advantage of being able to use low cost induction machines, are still limited to the lower end of the high power range due to the limitations on the gate-turn-off type semiconductor power device ratings.

In the past decade, multi-level inverter fed electric machine drive systems have emerged as a promising approach in achieving high power ratings with voltage limited devices. The typical structure of such systems is the three-level inverter three-phase electric machine system [1]. A three-level voltage source inverter is a series switch type structure which operates with split-voltage dc bus. The voltage stress on each device is only half of the total dc bus voltage and, thus, a doubled dc bus voltage can be achieved. The parallel circuit dual to the multi-level system is, essentially, the concept of the multi-phase inverter fed electric machine drive system. In a multi-phase machine drive system, more than three phase windings are implemented in the same stator of the electric machine, and the current per phase in the machine is thereby reduced. In the most common such structure, two sets of three-phase windings are spatially phase shifted by 30 electrical degrees. In such systems, each set of the three-phase stator windings is excited by a three-phase inverter, therefore the total power rating of the system is doubled. In addition to enhancing power rating, it is also believed that drive systems with such multi-phase redundant structure will improve the reliability at the system level [2], [3]. In particular, unlike in a normal three phase system, the loss of one phase in a multi-phase machine drive system does not prevent the machine from starting and running.

However, when a multi-phase system is implemented with a voltage source inverter with conventional six-step operation or space vector PWM control, surprisingly large harmonic currents have been observed [4]–[6]. Although this peculiarity has drawn attention from people working on this kind of system, little work has been done in developing a dedicated control strategy to effectively suppress the harmonics due to the complexity of the converter-machine model.

It is well known that the d-q-0 reference frame transformation has long been used successfully in the analysis and control of three-phase electric machines. In this technology, the original three-dimensional vector space is decomposed into the direct sum of a d-q subspace and a zero sequence subspace, which is orthogonal to the d-q. By virtue of this decomposition, the components which produce rotating MMF and the components of zero sequence are totally decoupled, and thus the analysis and the control of the machine is simplified.

For the analysis of multi-phase machines, a variety of transformations has been proposed in the past [5]–[10]. Symmetrical component theory and matrix theory have served as the theoretical foundations for these transformations. In this paper, matrix theory and the concept of decomposition are adopted in developing a transformation for dual three-phase induction machines. A companion vector space decomposition control technique is also proposed. By vector space decomposition, the machine current and voltage vectors in the original six-dimensional vector space are mapped into three two-dimensional orthogonal subspaces. As a result, the machine model can be easily described by three sets of decoupled equations. The techniques presented in this paper can also be used to analyze the current source inverter fed dual three-phase machines and generalized to control multi-phase induction machine drive systems.

Paper IPCSD 95–25, approved by the Industrial Drives Committee of the IEEE Industry Applications Society for presentation at the 1994 IEEE Industry Applications Society Annual Meeting, Denver, CO, October 2–7. This work received support from the Electric Power Research Institute. Manuscript released for publication March 10, 1995.

The authors are with the Department of Electrical and Computer Engineering, University of Wisconsin, Madison, WI 53706 USA.

IEEE Log Number 9412784.

II. Vector Space Decomposition and Transformation Matrix

Since six independent currents can flow in the general case, a dual three-phase induction machine is basically a six-dimensional system. Therefore, the modeling and control problems of such systems must be addressed from the point of view of a six-dimensional space. Consider, for example, the dual three-phase induction machine drive system in Fig. 1 and assume that the six-phase voltage or current variables are being sampled at some instant of time. The set of the sampled data x, which can be either voltage or current, can be represented as a vector in a six-dimensional space as

$$\begin{bmatrix} x_a \\ x_b \\ x_c \\ x_d \\ x_e \\ x_f \end{bmatrix}, \text{ here the standard basis vector set}$$

$$e_1 = \begin{bmatrix} 1 \\ 0 \\ 0 \\ 0 \\ 0 \\ 0 \end{bmatrix}, \ldots, \quad e_6 = \begin{bmatrix} 0 \\ 0 \\ 0 \\ 0 \\ 0 \\ 1 \end{bmatrix} \text{ is implied.}$$

As the variables are functions of time, the vector rotates about the origin and spans a surface in the six-dimensional space. Geometrically, the proper control of the dual three-phase machine is equivalent to positioning the vector on a certain surface in the six-dimensional vector space and rotating this vector at a desired speed. This requirement makes the modeling and control of the dual three-phase machine very difficult. However, the modeling and control of the dual three-phase induction machine can be greatly simplified with a proper transformation which maps the description of a vector with respect to the original six-dimensional frame spanned by the six standard base vectors to a new reference frame. For doing so, a set of six vectors should be chosen to form the new base of the six-dimensional space, and, for purpose of decomposition, it is desirable that the six vectors be orthogonal each other.

For the dual three-phase induction machine in Fig. 1, suitable voltage and current vectors can be evolved by defining the following vector:

$$\begin{aligned} \mathcal{S}_k(\omega t) = [&\cos k(\omega t), \cos k(\omega t - \theta), \\ &\cos k(\omega t - 4\theta), \cos k(\omega t - 5\theta), \\ &\cos k(\omega t - 8\theta), \cos k(\omega t - 9\theta)]^T \end{aligned} \quad (1)$$

where $\theta = \pi/6$, and $k = 0, 1, 3, 5, \ldots$, which denotes the order of the time harmonics. As the elements of the vectors are functions of time, each vector spans a two-dimensional surface, which can be proven to be a subspace in the original six-dimensional space.

The surface spanned by the fundamental component vector is of key importance to the electromechanical energy conversion function of the machine. Therefore, two out of the six new base vectors must be chosen from this surface. Let

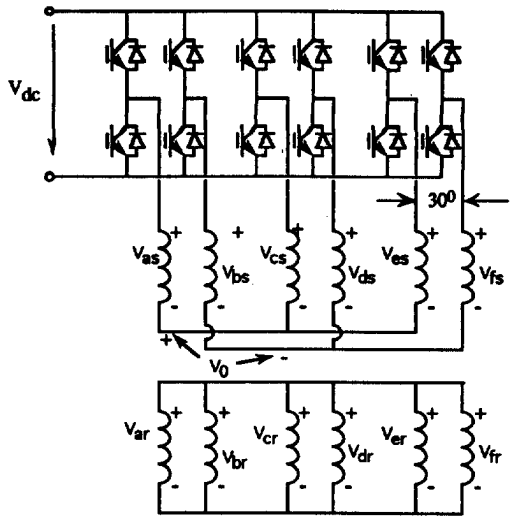

Fig. 1. Voltage source inverter fed dual three-phase induction machine drive system.

$k = 1$ in (1), and $\omega t = 0$ and $\pi/2$ to make the resultant vectors orthogonal. Two vectors, named d and q, are obtained as shown below

$$\begin{aligned} d&: [1, \cos(\theta), \cos(4\theta), \cos(5\theta), \cos(8\theta), \cos(9\theta)]^T, \\ &(\omega t = 0) \\ q&: [0, \sin(\theta), \sin(4\theta), \sin(5\theta), \sin(8\theta), \sin(9\theta)]^T, \\ &(\omega t = \pi/2). \end{aligned}$$

As pointed out before, the rest of the four vectors should be selected such that they are orthogonal each other and also orthogonal to vectors d and q. To find these four vectors the relations between the surfaces $\mathcal{S}_k$, which are spanned by a different order of harmonics when $k\omega t$ changes from 0 to 2π, are examined and it is found that the surfaces corresponding to $k = 1, 3, 5$ are orthogonal each other, i.e.

$$\mathcal{S}_1^T \bullet \mathcal{S}_3 = \mathcal{S}_1^T \bullet \mathcal{S}_5 = \mathcal{S}_3^T \bullet \mathcal{S}_5 = 0 \quad (0 \le \omega t \le 2\pi).$$

Surfaces spanned by harmonics of higher order ($k = 7, 9$, etc.) can be shown to generate the same surfaces as the $k = 1, 3, 5$ surfaces. Therefore, with two orthogonal vectors being selected from each of the two surfaces as indicated below, the orthogonality of the new base vector set is guaranteed.

With $k = 5$ we have

$$\begin{aligned} z_1&: [1, \cos(5\theta), \cos(8\theta), \cos(\theta), \cos(4\theta), \cos(9\theta)]^T, \\ &(\omega t = 0) \\ z_2&: [0, \sin(5\theta), \sin(8\theta), \sin(\theta), \sin(4\theta), \sin(9\theta)]^T, \\ &(\omega t = \pi/2). \end{aligned}$$

With $k = 3$ we have

$$\begin{aligned} o_1&: [1, 0, 1, 0, 1, 0]^T, \quad (\omega t = 0) \\ o_2&: [0, 1, 0, 1, 0, 1]^T, \quad (\omega t = \pi/6). \end{aligned}$$

With these six vectors used as the new basis of the six-dimensional space, the following normalized coordinate transformation matrix results (see (2), shown at the bottom of the following page).

The transformation possesses the following properties:

1) The fundamental component of the machine variables and the kth order harmonics with $k = 12m \pm 1$, $(m = 1, 2, 3, \ldots)$ are transformed into the d-q subspace or 'd-q plane.

   It should be pointed out that the d-q axes have been chosen in such a manner that they coincide with the plane of rotation of the air gap flux. Therefore, these variables will produce a rotating MMF in the machine airgap and thus be electromechanical energy conversion related.
2) Harmonics with $k = 6m \pm 1, (m = 1, 3, 5, \ldots)$, i.e., the 5th, 7th, 17th, 19th, ... harmonics, are mapped into the z_1-z_2 subspace, or "z_1-z_2 plane." As the z_1-z_2 subspace is orthogonal to the d-q subspace, it is expected that the variables on this plane will not generate any rotating MMF in the airgap and thus be nonelectromechanical energy conversion related. In this regard, these harmonics can be classified as a new type of zero sequence component.
3) Zero sequence $(m - 3)$ harmonics, which are also nonelectromechanical energy conversion related, are mapped into the 0_1-0_2 subspace to form the conventional zero sequence components.

III. Machine Model

The following assumptions have been made in deriving the dual three-phase induction machine model:

1) Machine windings are sinusoidally distributed.
2) Flux path is linear.
3) Mutual leakage inductances are neglected.
4) Assume unity stator and rotor turn ratio.

Under these assumptions the voltage equations of the machine in the original six-dimensional space and the equations transformed to the d-q-z_1-z_2-0_1-0_2 reference frame can be derived.

A. Machine Model in the Original Six-Dimensional Space

The stator voltage equation is

$$\begin{aligned}[V_s] &= [R_s] \cdot [i_s] + p \cdot ([\lambda_s]) \\ &= [R_s] \cdot [i_s] + p \cdot ([\lambda_{ss}] + [\lambda_{sr}]) \\ &= [R_s] \cdot [i_s] + p \cdot ([L_{ss}] \cdot [i_s] + [L_{sr}] \cdot [i_r]). \end{aligned} \quad (3)$$

The rotor voltage equation is

$$\begin{aligned}[V_r] &= [R_r] \cdot [i_r] + p \cdot ([\lambda_r]) \\ &= [R_r] \cdot [i_r] + p \cdot ([\lambda_{rr}] + [\lambda_{rs}]) \\ &= [R_r] \cdot [i_r] + p \cdot ([L_{rr}] \cdot [i_r] + [L_{rs}] \cdot [i_s]) \end{aligned} \quad (4)$$

where, in these equations, the voltage and current vectors are defined as

$$[v_s] = \begin{bmatrix} v_{as} \\ v_{bs} \\ v_{cs} \\ v_{ds} \\ v_{es} \\ v_{fs} \end{bmatrix}, \quad [i_s] = \begin{bmatrix} i_{as} \\ i_{bs} \\ i_{cs} \\ i_{ds} \\ i_{es} \\ i_{fs} \end{bmatrix},$$

$$[v_r] = \begin{bmatrix} 0 \\ 0 \\ 0 \\ 0 \\ 0 \\ 0 \end{bmatrix}, \quad [i_r] = \begin{bmatrix} i_{ar} \\ i_{br} \\ i_{cr} \\ i_{dr} \\ i_{er} \\ i_{fr} \end{bmatrix}.$$

The resistance and inductance matrices in (3) and (4) are defined as follows according to the machine structure: $[R_s], [R_r]$ are the stator and rotor resistance matrices

$$[R_s] = \begin{bmatrix} r_s & 0 & 0 & 0 & 0 & 0 \\ 0 & r_s & 0 & 0 & 0 & 0 \\ 0 & 0 & r_s & 0 & 0 & 0 \\ 0 & 0 & 0 & r_s & 0 & 0 \\ 0 & 0 & 0 & 0 & r_s & 0 \\ 0 & 0 & 0 & 0 & 0 & r_s \end{bmatrix},$$

$$[R_r] = \begin{bmatrix} r_r & 0 & 0 & 0 & 0 & 0 \\ 0 & r_r & 0 & 0 & 0 & 0 \\ 0 & 0 & r_r & 0 & 0 & 0 \\ 0 & 0 & 0 & r_r & 0 & 0 \\ 0 & 0 & 0 & 0 & r_r & 0 \\ 0 & 0 & 0 & 0 & 0 & r_r \end{bmatrix}.$$

$[L_{ss}]$ is the stator self inductance matrix

$$[L_{ss}] = L_{ls} \begin{bmatrix} 1 & 0 & 0 & 0 & 0 & 0 \\ 0 & 1 & 0 & 0 & 0 & 0 \\ 0 & 0 & 1 & 0 & 0 & 0 \\ 0 & 0 & 0 & 1 & 0 & 0 \\ 0 & 0 & 0 & 0 & 1 & 0 \\ 0 & 0 & 0 & 0 & 0 & 1 \end{bmatrix} + L_{ms} \begin{bmatrix} 1 & \frac{\sqrt{3}}{2} & -\frac{1}{2} & -\frac{\sqrt{3}}{2} & -\frac{1}{2} & 0 \\ \frac{\sqrt{3}}{2} & 1 & 0 & -\frac{1}{2} & -\frac{\sqrt{3}}{2} & -\frac{1}{2} \\ -\frac{1}{2} & 0 & 1 & \frac{\sqrt{3}}{2} & -\frac{1}{2} & -\frac{\sqrt{3}}{2} \\ -\frac{\sqrt{3}}{2} & -\frac{1}{2} & \frac{\sqrt{3}}{2} & 1 & 0 & -\frac{1}{2} \\ -\frac{1}{2} & -\frac{\sqrt{3}}{2} & -\frac{1}{2} & 0 & 1 & \frac{\sqrt{3}}{2} \\ 0 & -\frac{1}{2} & -\frac{\sqrt{3}}{2} & -\frac{1}{2} & \frac{\sqrt{3}}{2} & 1 \end{bmatrix}$$

where L_{ls} and L_{ms} are the stator leakage and magnetizing inductance.

$$[T] = \frac{1}{\sqrt{3}} \begin{bmatrix} 1 & \cos(\theta) & \cos(4\theta) & \cos(5\theta) & \cos(8\theta) & \cos(9\theta) \\ 0 & \sin(\theta) & \sin(4\theta) & \sin(5\theta) & \sin(8\theta) & \sin(9\theta) \\ 1 & \cos(5\theta) & \cos(8\theta) & \cos(\theta) & \cos(4\theta) & \cos(9\theta) \\ 0 & \sin(5\theta) & \sin(8\theta) & \sin(\theta) & \sin(4\theta) & \sin(9\theta) \\ 1 & 0 & 1 & 0 & 1 & 0 \\ 0 & 1 & 0 & 1 & 0 & 1 \end{bmatrix}. \quad (2)$$

Shown at the bottom of the page are

$[L_{rr}]$ rotor self inductance matrix where L_{lr} is the rotor leakage inductance,

$[L_{\rm sr}]$ stator-rotor mutual inductance matrix where θ_r is the rotor angular position,

$[L_{\rm rs}]$ rotor-stator mutual inductance matrix.

B. Transformation of the Voltage Equations to the New Reference Frame

Applying the transformation (2) to the voltage equations (3) and (4) yields

$$\begin{aligned}[T]\cdot[V_s] &= [T]\cdot[R_s]\cdot[T^{-1}]\cdot[T]\cdot[i_s] \\ &\quad + p\cdot\left([T]\cdot[L_{\rm ss}]\cdot[T]^{-1}\cdot[T]\cdot[i_s]\right. \\ &\quad \left.+[T]\cdot[L_{\rm sr}]\cdot[T]^{-1}\cdot[T]\cdot[i_r]\right) \qquad (5) \\ [T]\cdot[V_r] &= [T]\cdot[R_r]\cdot[T^{-1}]\cdot[T]\cdot[i_r] \\ &\quad + p\cdot\left([T]\cdot[L_{rr}]\cdot[T]^{-1}\cdot[T]\cdot[i_r]\right. \\ &\quad \left.+[T]\cdot[L_{\rm rs}]\cdot[T]^{-1}\cdot[T]\cdot[i_s]\right) \qquad (6)\end{aligned}$$

where in (6), the voltage and current vectors transformed to the new d-q-z_1-z_2-0_1-0_2 reference frame are defined as

$$\begin{bmatrix} v_{ds} \\ v_{qs} \\ v_{z_1 s} \\ v_{z_2 s} \\ v_{0_1 s} \\ v_{0_2 s}\end{bmatrix} = [T]\cdot[v_s], \quad \begin{bmatrix} i_{ds} \\ i_{qs} \\ i_{z_1 s} \\ i_{z_2 s} \\ i_{0_1 s} \\ i_{0_2 s}\end{bmatrix} = [T]\cdot[i_s],$$

$$\begin{bmatrix} v_{dr} \\ v_{qr} \\ v_{z_1 r} \\ v_{z_2 r} \\ v_{0_1 r} \\ v_{0_2 r}\end{bmatrix} = [T]\cdot[v_r] = \begin{bmatrix}0\\0\\0\\0\\0\\0\end{bmatrix}, \begin{bmatrix} i_{dr} \\ i_{qr} \\ i_{z_1 r} \\ i_{z_2 r} \\ i_{0_1 r} \\ i_{0_2 r}\end{bmatrix} = [T]\cdot[i_r].$$

The subscript ds is now, in this case, intended to denote the stator d-axis and not phase ds as in Figs. 1 and 2. The dynamic models of the machine in the three subspaces can be derived from (6) and are illustrated as follows.

Machine model in d-q subspace:

The stator voltage equation is

$$\begin{aligned}\begin{bmatrix} v_{ds} \\ v_{\rm qs}\end{bmatrix} &= \begin{bmatrix} r_s & 0 \\ 0 & r_s\end{bmatrix}\cdot\begin{bmatrix} i_{ds} \\ i_{qs}\end{bmatrix} \\ &\quad + \frac{d}{dt}\left\{\begin{bmatrix} L_{ls}+3L_{ms} & 0 \\ 0 & L_{ls}+3L_{ms}\end{bmatrix}\cdot\begin{bmatrix} i_{ds} \\ i_{\rm qs}\end{bmatrix}\right. \\ &\quad \left.+L_{ms}\begin{bmatrix}3\cos(\theta_r) & -3\sin(\theta_r) \\ 3\sin(\theta_r) & \cos(\theta_r)\end{bmatrix}\cdot\begin{bmatrix} i_{dr} \\ i_{qr}\end{bmatrix}\right\}. \qquad (7)\end{aligned}$$

The rotor voltage equation is

$$\begin{aligned}\begin{bmatrix}0\\0\end{bmatrix} &= \begin{bmatrix} r_r & 0 \\ 0 & r_r\end{bmatrix}\cdot\begin{bmatrix} i_{dr} \\ i_{qr}\end{bmatrix} \\ &\quad + \frac{d}{dt}\left\{\begin{bmatrix} L_{lr}+3L_{ms} & 0 \\ 0 & L_{lr}+3L_{ms}\end{bmatrix}\right. \\ &\quad \left.\cdot\begin{bmatrix} i_{dr} \\ i_{\rm qr}\end{bmatrix} + \frac{N_r}{N_s}L_{ms}\begin{bmatrix}3\cos(\theta_r) & 3\sin(\theta_r) \\ -3\sin(\theta_r) & \cos(\theta_r)\end{bmatrix}\cdot\begin{bmatrix} i_{ds} \\ i_{qs}\end{bmatrix}\right\}. \qquad (8)\end{aligned}$$

$$[L_{rr}] = L_{lr}\begin{bmatrix}1&0&0&0&0&0\\0&1&0&0&0&0\\0&0&1&0&0&0\\0&0&0&1&0&0\\0&0&0&0&1&0\\0&0&0&0&0&1\end{bmatrix} + L_{ms}\begin{bmatrix} 1 & \frac{\sqrt{3}}{2} & -\frac{1}{2} & -\frac{\sqrt{3}}{2} & -\frac{1}{2} & 0 \\ \frac{\sqrt{3}}{2} & 1 & 0 & -\frac{1}{2} & -\frac{\sqrt{3}}{2} & -\frac{1}{2} \\ -\frac{1}{2} & 0 & 1 & \frac{\sqrt{3}}{2} & -\frac{1}{2} & -\frac{\sqrt{3}}{2} \\ -\frac{\sqrt{3}}{2} & -\frac{1}{2} & \frac{\sqrt{3}}{2} & 1 & 0 & -\frac{1}{2} \\ -\frac{1}{2} & -\frac{\sqrt{3}}{2} & -\frac{1}{2} & 0 & 1 & \frac{\sqrt{3}}{2} \\ 0 & -\frac{1}{2} & -\frac{\sqrt{3}}{2} & -\frac{1}{2} & \frac{\sqrt{3}}{2} & 1 \end{bmatrix}.$$

$$[L_{\rm sr}] = L_{ms}\begin{bmatrix} \cos(\theta_r) & \cos(\frac{\pi}{6}+\theta_r) & \cos(\frac{4\pi}{6}+\theta_r) & \cos(\frac{5\pi}{6}+\theta_r) & \cos(\frac{8\pi}{6}+\theta_r) & \cos(\frac{9\pi}{6}+\theta_r) \\ \cos(\frac{11\pi}{6}+\theta_r) & \cos(\theta_r) & \cos(\frac{3\pi}{6}+\theta_r) & \cos(\frac{4\pi}{6}+\theta_r) & \cos(\frac{7\pi}{6}+\theta_r) & \cos(\frac{8\pi}{6}+\theta_r) \\ \cos(\frac{8\pi}{6}+\theta_r) & \cos(\frac{9\pi}{6}+\theta_r) & \cos(\theta_r) & \cos(\frac{\pi}{6}+\theta_r) & \cos(\frac{4\pi}{6}+\theta_r) & \cos(\frac{5\pi}{6}+\theta_r) \\ \cos(\frac{7\pi}{6}+\theta_r) & \cos(\frac{8\pi}{6}+\theta_r) & \cos(\frac{11\pi}{6}+\theta_r) & \cos(\theta_r) & \cos(\frac{3\pi}{6}+\theta_r) & \cos(\frac{4\pi}{6}+\theta_r) \\ \cos(\frac{4\pi}{6}+\theta_r) & \cos(\frac{5\pi}{6}+\theta_r) & \cos(\frac{8\pi}{6}+\theta_r) & \cos(\frac{9\pi}{6}+\theta_r) & \cos(\theta_r) & \cos(\frac{\pi}{6}+\theta_r) \\ \cos(\frac{3\pi}{6}+\theta_r) & \cos(\frac{4\pi}{6}+\theta_r) & \cos(\frac{7\pi}{6}+\theta_r) & \cos(\frac{8\pi}{6}+\theta_r) & \cos(\frac{11\pi}{6}+\theta_r) & \cos(\theta_r) \end{bmatrix}.$$

$$[L_{\rm rs}] = L_{ms}\begin{bmatrix} c(\theta_r) & c(\frac{\pi}{6}-\theta_r) & c(\frac{4\pi}{6}-\theta_r) & c(\frac{5\pi}{6}-\theta_r) & c(\frac{8\pi}{6}-\theta_r) & c(\frac{9\pi}{6}-\theta_r) \\ c(\frac{11\pi}{6}-\theta_r) & c(\theta_r) & c(\frac{3\pi}{6}-\theta_r) & c(\frac{4\pi}{6}-\theta_r) & c(\frac{7\pi}{6}-\theta_r) & c(\frac{8\pi}{6}-\theta_r) \\ c(\frac{8\pi}{6}-\theta_r) & c(\frac{9\pi}{6}-\theta_r) & c(\theta_r) & c(\frac{\pi}{6}-\theta_r) & c(\frac{4\pi}{6}-\theta_r) & c(\frac{5\pi}{6}-\theta_r) \\ c(\frac{7\pi}{6}-\theta_r) & c(\frac{8\pi}{6}-\theta_r) & c(\frac{11\pi}{6}-\theta_r) & c(\theta_r) & c(\frac{3\pi}{6}-\theta_r) & c(\frac{4\pi}{6}-\theta_r) \\ c(\frac{4\pi}{6}-\theta_r) & c(\frac{5\pi}{6}-\theta_r) & c(\frac{8\pi}{6}-\theta_r) & c(\frac{9\pi}{6}-\theta_r) & c(\theta_r) & c(\frac{\pi}{6}-\theta_r) \\ c(\frac{3\pi}{6}-\theta_r) & c(\frac{4\pi}{6}-\theta_r) & c(\frac{7\pi}{6}-\theta_r) & c(\frac{8\pi}{6}-\theta_r) & c(\frac{11\pi}{6}-\theta_r) & c(\theta_r) \end{bmatrix}.$$

Machine model in z_1-z_2 subspace:
The stator equation is

$$\frac{d}{dt}\begin{bmatrix} i_{z_1 s} \\ i_{z_2 s} \end{bmatrix} = \begin{bmatrix} -r_s/L_{ls} & 0 \\ 0 & -r_s/L_{ls} \end{bmatrix} \cdot \begin{bmatrix} i_{z_1 s} \\ i_{z_2 s} \end{bmatrix} + \begin{bmatrix} 1/L_{ls} & 0 \\ 0 & 1/L_{ls} \end{bmatrix} \cdot \begin{bmatrix} v_{z_1 s} \\ v_{z_2 s} \end{bmatrix}. \tag{9}$$

The rotor equation is

$$\frac{d}{dt}\begin{bmatrix} i_{z_1 r} \\ i_{z_2 r} \end{bmatrix} = \begin{bmatrix} -r_r/L_{lr} & 0 \\ 0 & -r_r/L_{lr} \end{bmatrix} \cdot \begin{bmatrix} i_{z_1 r} \\ i_{z_2 r} \end{bmatrix}. \tag{9a}$$

Machine model in 0_1-0_2 subspace:
The stator equation is

$$\frac{d}{dt}\begin{bmatrix} i_{0_1 s} \\ i_{0_2 s} \end{bmatrix} = \begin{bmatrix} -r_s/L_{ls} & 0 \\ 0 & -r_s/L_{ls} \end{bmatrix} \cdot \begin{bmatrix} i_{0_1 s} \\ i_{0_2 s} \end{bmatrix} + \begin{bmatrix} 1/L_{ls} & 0 \\ 0 & 1/L_{ls} \end{bmatrix} \cdot \begin{bmatrix} v_{0_1 s} \\ v_{0_2 s} \end{bmatrix}. \tag{10}$$

The rotor equation is

$$\frac{d}{dt}\begin{bmatrix} i_{0_1 r} \\ i_{0_2 r} \end{bmatrix} = \begin{bmatrix} -r_r/L_{lr} & 0 \\ 0 & -r_r/L_{lr} \end{bmatrix} \cdot \begin{bmatrix} i_{0_1 r} \\ i_{0_2 r} \end{bmatrix}. \tag{10a}$$

It is observed that the stator equations in the z_1-z_2 and the 0_1-0_2 subspaces have the same form and the same parameters. This is due to the assumption that the stator mutual leakage inductances can be ignored. With mutual leakage inductance considered, the leakage inductances in (9) and (10) will have different values. The effect of the mutual leakage inductances will be addressed in the future research work on this machine. It is also observed that there are no excitation terms in (9a) and (10a). Therefore, this portion of the machine dynamics can never be excited and, hence, will not be discussed further in this paper.

It is observed immediately from the above equations that all the electromechanical energy conversion related variable components are mapped into the d-q subspace, or "d-q-plane," and the nonelectromechanical energy conversion related variable components are transformed to the z_1-z_2 and 0_1-0_2 planes. Hence, the dynamic equations of the machine are totally decoupled. As a result, the analysis and control of the machine can be greatly simplified.

It is also important to note that the nonelectromechanical energy conversion related variables on the z_1-z_2 and the o_1-o_2 planes should be controlled to be as small as possible to reduce the extra losses in the machine. However, as can be seen from (9) and (10), only stator resistance and leakage inductance are associated with these variables. As a result, high switching frequency inverters are generally required in a voltage source inverter fed multi-phase induction machine drive. This, clearly, is a drawback of such a system.

In the analysis just completed, d-q reference frames were, in effect, separately attached to the stator and the rotor, rotating at zero and rotor angular speed, respectively. To express the stator and rotor equations in the same stationary reference frame and thus eliminate the sin and the cos terms in the above equations, the following rotation transformation, which transforms the rotor variables to the stationary reference frame, is appropriate

$$[T_r^s] = \begin{bmatrix} \cos(\theta_r) & -\sin(\theta_r) \\ \sin(\theta_r) & \cos(\theta_r) \end{bmatrix}. \tag{11}$$

Since both stator and rotor variables are expressed in the same reference frame now, it is necessary to distinguish them with a newly defined variable expression

$$\text{variable}^{\text{stator or rotor frame}}_{\text{d-or q-axis stator or rotor variable.}}$$

With the rotation transformation applied to (7) and (8), the following stator and rotor combined d-q plane stationary reference frame equation results:

$$\begin{bmatrix} v_{ds}^s \\ v_{qs}^s \\ 0 \\ 0 \end{bmatrix} = \begin{bmatrix} r_s + L_s p & 0 & Mp & 0 \\ 0 & r_s + L_s p & 0 & Mp \\ Mp & \omega_r M & r_r + L_r P & \omega_r L_r \\ -\omega_r M & Mp & -\omega_r L_r & r_r + L_r P \end{bmatrix} \cdot \begin{bmatrix} i_{ds}^s \\ i_{qs}^s \\ i_{dr}^s \\ i_{qr}^s \end{bmatrix} \tag{12}$$

where

$$p = \frac{d}{dt}$$
$$L_s = L_{ls} + 3L_{ms},$$
$$L_r = L_{lr} + 3L_{ms},$$
$$M = 3L_{ms}.$$

The electromagnetic torque of electric machine is expressed as

$$T_e = \frac{1}{2}[i]^T \cdot \left(\frac{\partial}{\partial \theta_r}[L]\right) \cdot [i]. \tag{13}$$

As the d-q plane is electromechanical energy conversion related, the current vector in (13) should include d-q plane currents only, i.e.

$$[i] = \begin{bmatrix} i_{ds}^s \\ i_{qs}^s \\ i_{dr}^r \\ i_{qr}^r \end{bmatrix}. \tag{14}$$

For the same reason, the d-q plane inductance matrix as illustrated in (15) should be used for the matrix $[L]$ in (13).

$$[L] = \begin{bmatrix} L_{ds,ds} & L_{ds,qs} & L_{ds,dr} & L_{ds,qr} \\ L_{qs,ds} & L_{qs,qs} & L_{qs,dr} & L_{qs,qr} \\ L_{dr,ds} & L_{dr,qs} & L_{dr,dr} & L_{dr,qr} \\ L_{qr,ds} & L_{qr,qs} & L_{qr,dr} & L_{qr,qr} \end{bmatrix} = \begin{bmatrix} L_s & 0 & M\cos(\theta_r) & -M\sin(\theta_r) \\ 0 & L_s & M\sin(\theta_r) & M\cos(\theta_r) \\ M\cos(\theta_r) & M\sin(\theta_r) & L_r & 0 \\ -M\sin(\theta_r) & M\cos(\theta_r) & 0 & L_r \end{bmatrix}. \tag{15}$$

The electromagnetic torque of the dual three phase induction machine is obtained by substituting (14) and (15) into (13) as

$$\begin{aligned} T_e &= 3L_{ms}[i^s_{qs}(r^r_{dr}\cos(\theta_r) - r^r_{qr}\sin(\theta_r)) \\ &\qquad - i^s_{ds}(r^r_{dr}\sin(\theta_r) + r^r_{qr}\cos(\theta_r))] \\ &= 3L_{ms}(i^s_{qs}i^s_{dr} - i^s_{ds}i^s_{qr}). \end{aligned} \tag{16}$$

When the number of poles is greater than two

$$T_e = 3\frac{P}{2}L_{ms}(i^s_{qs}i^s_{dr} - i^s_{ds}i^s_{qr}). \tag{17}$$

P is the machine pole number.

IV. Space Vector PWM Control Strategy

In the dual three-phase machine drive system shown in Fig. 1, the stator windings can be connected either to a single neutral or to double neutrals. Neutral wires eliminated in both cases will clearly reduce the dimension of the system.

In general, the six-phase voltage source inverter has a total of 64 switching modes. By using the transformation matrix (2), the 64 voltage vectors corresponding to the switching modes are projected on the three planes. A space vector PWM control strategy which covers the control of the volt-seconds applied to the machine in all the three planes will now be developed.

A. Transformation of the Inverter Output Voltage Vectors to the d-q-z_1-z_2-0_1-0_2 Reference Frame

With the machine stator windings connected to the inverter without a neutral wire, only the line voltages of the machine corresponding to the inverter switching modes are directly known. On the other hand, the transformation matrix (2) transforms the machine phase variables to the new d-q-z_1-z_2-0_1-0_2 reference frame. Therefore, it is necessary to develop transformations from line voltages to phase voltages.

Fig. 2 shows two cases for the stator winding neutral point connection. In Fig. 2(a), the stator windings are connected to a single neutral, the relation between the line and the phase voltages are defined by a full rank matrix as illustrated in (18).

$$\begin{bmatrix} v_{abs} \\ v_{bcs} \\ v_{cds} \\ v_{des} \\ v_{efs} \\ 0 \end{bmatrix} = \begin{bmatrix} 1 & -1 & 0 & 0 & 0 & 0 \\ 0 & 1 & -1 & 0 & 0 & 0 \\ 0 & 0 & 1 & -1 & 0 & 0 \\ 0 & 0 & 0 & 1 & -1 & 0 \\ 0 & 0 & 0 & 0 & 1 & -1 \\ 1 & 1 & 1 & 1 & 1 & 1 \end{bmatrix} \cdot \begin{bmatrix} v_{as} \\ v_{bs} \\ v_{cs} \\ v_{ds} \\ v_{es} \\ v_{fs} \end{bmatrix}. \tag{18}$$

The transformation from line voltage to phase voltage can be derived from (18) by inverting the matrix. The resultant transformation is shown in (19).

$$\begin{bmatrix} v_{as} \\ v_{bs} \\ v_{cs} \\ v_{ds} \\ v_{es} \\ v_{fs} \end{bmatrix} = \frac{1}{6}\begin{bmatrix} 5 & 4 & 3 & 2 & 1 & 1 \\ -1 & 4 & 3 & 2 & 1 & 1 \\ -1 & -2 & 3 & 2 & 1 & 1 \\ -1 & -2 & -3 & 2 & 1 & 1 \\ -1 & -2 & -3 & -4 & 1 & 1 \\ -1 & -2 & -3 & -4 & -5 & 1 \end{bmatrix} \cdot \begin{bmatrix} v_{abs} \\ v_{bcs} \\ v_{cds} \\ v_{des} \\ v_{efs} \\ 0 \end{bmatrix}. \tag{19}$$

Similarly, the transformation for the case of double neutral connection (see Fig. 2(b)) can be derived and illustrated in (20) and (21).

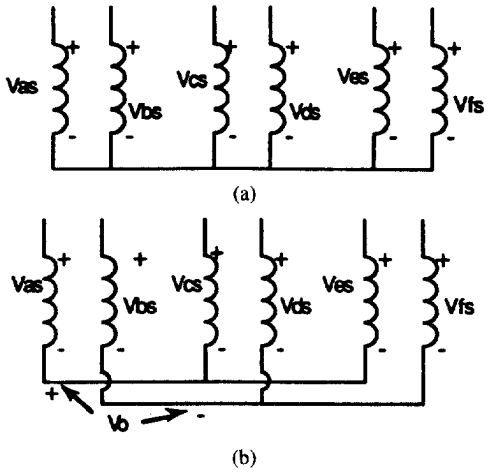

Fig. 2. Stator winding connection. (a) Single neutral point case. (b) Double neutral point case.

Phase voltage to line voltage transformation for double neutral connection

$$\begin{bmatrix} v_{abs} \\ v_{bcs} \\ v_{cds} \\ v_{des} \\ v_{efs} \\ 0 \\ 0 \end{bmatrix} = \begin{bmatrix} 1 & 1 & -1 & 0 & 0 & 0 & 0 \\ -1 & 0 & 1 & -1 & 0 & 0 & 0 \\ 1 & 0 & 0 & 1 & -1 & 0 & 0 \\ -1 & 0 & 0 & 0 & 1 & -1 & 0 \\ 1 & 0 & 0 & 0 & 0 & 1 & -1 \\ 0 & 1 & 0 & 1 & 0 & 1 & 0 \\ 0 & 0 & 1 & 0 & 1 & 0 & 1 \end{bmatrix} \begin{bmatrix} v_0 \\ v_{as} \\ v_{bs} \\ v_{cs} \\ v_{ds} \\ v_{es} \\ v_{fs} \end{bmatrix}. \tag{20}$$

Line voltage to phase voltage transformation for double neutral connection

$$\begin{bmatrix} v_0 \\ v_{as} \\ v_{bs} \\ v_{cs} \\ v_{ds} \\ v_{es} \\ v_{fs} \end{bmatrix} = \frac{1}{6}\begin{bmatrix} 2 & 0 & 2 & 0 & 2 & -2 & 2 \\ 4 & 4 & 2 & 2 & 0 & 2 & 0 \\ 0 & 4 & 4 & 2 & 2 & 0 & 2 \\ -2 & -2 & 2 & 2 & 0 & 2 & 0 \\ 0 & -2 & -2 & 2 & 2 & 0 & 2 \\ -2 & -2 & -4 & -4 & 0 & 2 & 0 \\ 0 & -2 & -2 & -4 & -4 & 0 & 2 \end{bmatrix} \begin{bmatrix} v_{abs} \\ v_{bcs} \\ v_{cds} \\ v_{des} \\ v_{efs} \\ 0 \\ 0 \end{bmatrix}. \tag{21}$$

The next step is to combine the transformation (2) with the transformation (19) or (21) to transform the inverter voltage vectors corresponding to the 64 switching modes to the d-q-z_1-z_2-0_1-0_2 reference frame.

When the stator windings are connected to single neutral, the inverter voltage vectors are transformed to all three planes as shown in Fig. 3(a)–(c). Note that all the voltage vectors on o_1-o_2 plane now lie on a straight line. Therefore, the system is, in actuality, five-dimensional.

The decimal numbers in the figures denote the switching modes. When each decimal number is converted to a six-digit binary number, the 1's in this number indicate that the upper switches in the corresponding switching arms are "on," while the 0's indicate the "on" state of the lower switches. The MSB (most significant bit) of the number represents the switching state of phase a, the second MSB for phase b, and so on.

In the case when the stator windings are connected to double neutrals as in Fig. 2(b), the projections of the inverter voltage vectors on the d-q, z_1-z_2 planes remain the same as in the single neutral case. However, on the 0_1-0_2 plane all the vectors

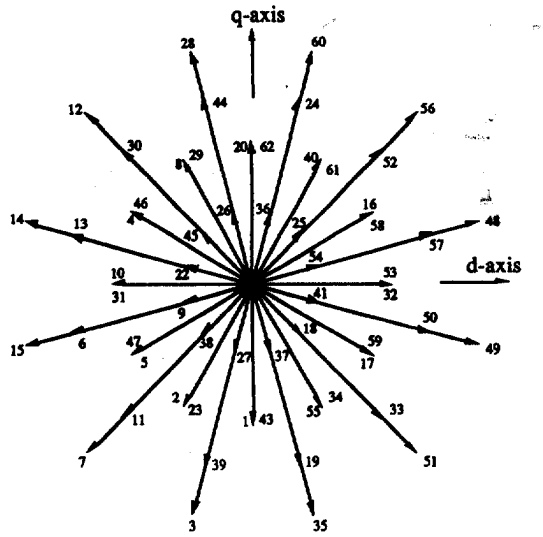

(a)

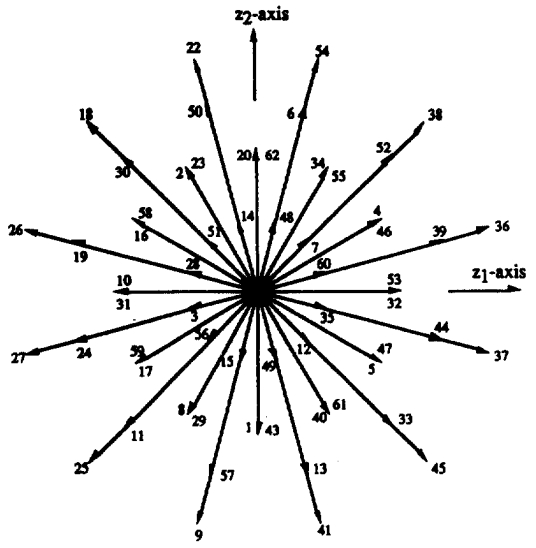

(b)

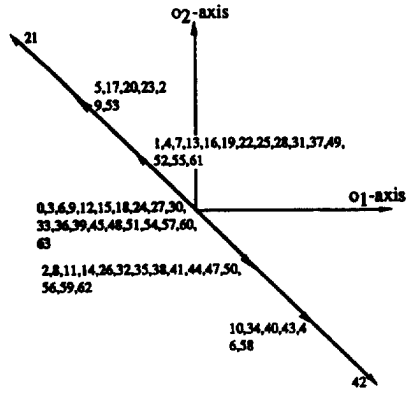

(c)

Fig. 3. (a) Inverter voltage vectors projected on d-q plane (switching modes at origin: 0, 21, 42, 63). (b) Inverter voltage vectors projected on z_1-z_2 plane (switching modes at origin: 0, 21, 42, 63). (c) Inverter voltage vectors projected on 0_1-0_2 plane.

are mapped to the origin. The resultant system is a four-dimensional system, and the control of the dual three-phase machine is further simplified.

B. Space Vector PWM Control

The machine model which has been developed has demonstrated that only the voltages and currents in the d-q plane are related to electromechanical energy conversion. Therefore, the goal of the space vector PWM control is to synthesize the d-q voltage vectors to satisfy the machine's torque control requirements, and, at the same time, to maintain the average volt-seconds on the z_1-z_2 and 0_1-0_2 planes to be zero during every sampling interval.

The space vector PWM strategy discussed in this paper is based on the double neutral topology as illustrated in Fig. 2(b). With stator windings connected to double neutrals, the projection of the current vector on the o_1-o_2 plane is inherently zero and the space vector PWM is performed only on the d-q and z_1-z_2 planes.

The space vector PWM strategy is accomplished by the following equation

$$\begin{bmatrix} T_1 \\ T_2 \\ T_3 \\ T_4 \\ T_5 \end{bmatrix} = \begin{bmatrix} v_d^1 & v_d^2 & v_d^3 & v_d^4 & v_d^5 \\ v_q^1 & v_q^2 & v_q^3 & v_q^4 & v_q^5 \\ v_{z_1}^1 & v_{z_1}^2 & v_{z_1}^3 & v_{z_1}^4 & v_{z_1}^5 \\ v_{z_2}^1 & v_{z_2}^2 & v_{z_2}^3 & v_{z_2}^4 & v_{z_2}^5 \\ 1 & 1 & 1 & 1 & 1 \end{bmatrix}^{-1} \cdot \begin{bmatrix} v_d^* T_s \\ v_q^* T_s \\ 0 \\ 0 \\ T_s \end{bmatrix} \quad (22)$$

where v_x^k is the projection of the kth voltage vector on the x-axis, and T_k is the dwell time of that vector during time interval T_s. The quantities v_d^* and v_q^* are the d-q plane reference voltages.

During each sampling period T_s, a set of five voltage vectors must be chosen to guarantee that each T_k has a positive and unique solution. There are numerous means for choosing such a set. The set used in this paper is illustrated in Fig. 4. In the method chosen, four adjacent voltage vectors are always selected from the vectors which span the outermost polygon on the d-q plane according to the position of the reference voltage vector V_{dq}^*. The fifth vector is chosen from the zero vectors located at the d-q plane origin. For example, as indicated by the dots in Fig. 4(a), voltage vectors 49, 48, 56, and 60 are selected when the reference voltage vector lies inside the triangle area between voltage vectors 48 and 56. In Fig. 4(b), the four voltage vectors spread out to cover the z_1-z_2 plane, thus making it possible that the average volt-second on this plane be zeroed during every sampling interval.

It is also noted from Fig. 4(b) that the vectors on the z_1-z_2 plane have the smallest amplitude. Therefore, the proposed space vector PWM strategy will offer the maximum voltage output capability on the d-q plane yet keep the harmonics on the z_1-z_2 plane at a minimum.

C. Simulation Results

The proposed vector space decomposition control technique has been simulated and the results are shown in Fig. 5. For purpose of comparison, the control using the conventional space vector PWM technique and sine-triangle PWM have also been simulated and the results are shown in Figs. 6 and 7. In all the simulations, the inverter switching frequencies were kept the same.

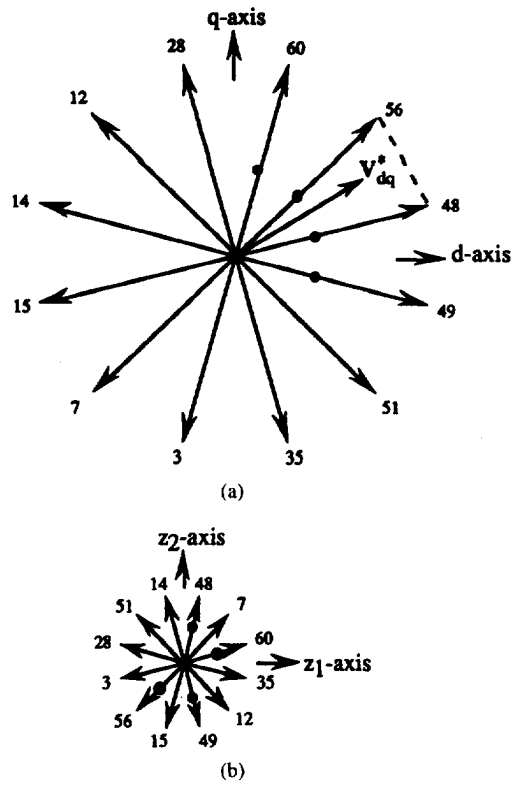

Fig. 4. Switching modes selection.

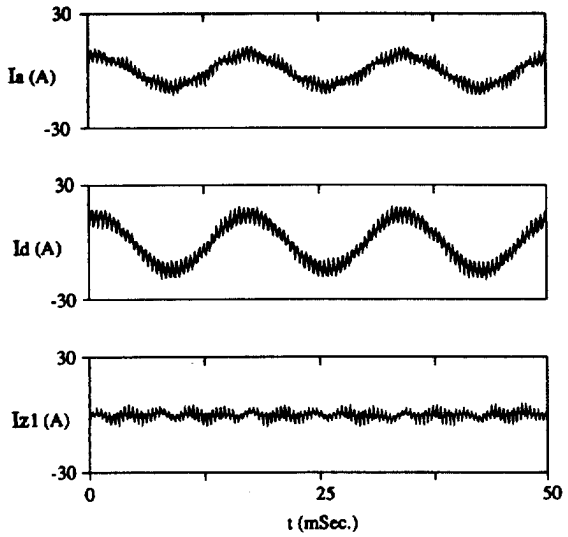

Fig. 5. Simulation result using proposed technique. From top to bottom: Machine phase current; current on d-q plane; and current on z_1-z_2 plane.

For the conventional space vector PWM, two adjacent voltage vectors plus one zero voltage vector at the origin are selected from the d-q plane. Since only the control over d-q plane variables is exercised, the harmonic currents on the z_1-z_2 plane are now left free to flow. As a result, the amplitudes of these currents will be expected to be quite large. Fig. 6 shows the simulation results for this case, where considerable large fifth and seventh harmonic currents can be observed.

The simulation results in Fig. 7 suggests that the sine-triangle PWM technique is superior for the control of the dual

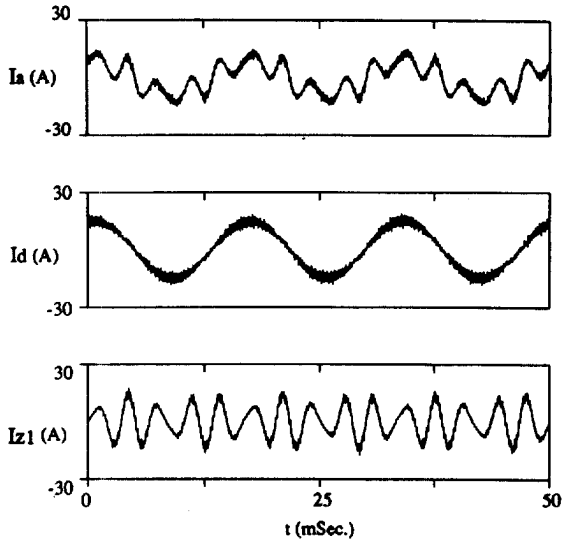

Fig. 6. Simulation result using conventional space vector PWM technique. From top to bottom: machine phase current, current on d-q plane, and current on z_1-z_2 plane.

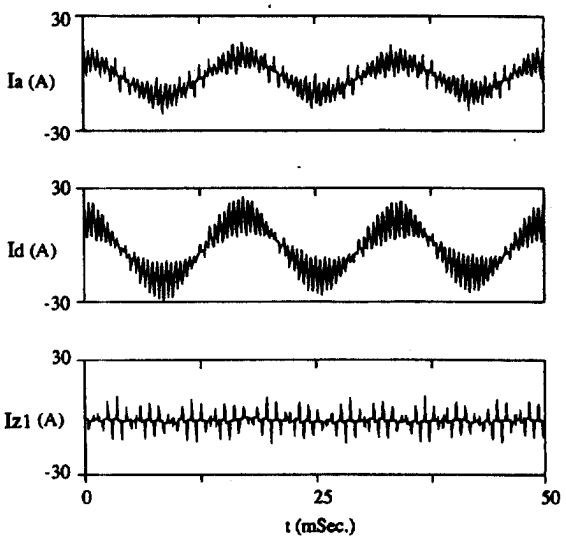

Fig. 7. Simulation result using sine-triangle PWM technique. From top to bottom: machine phase current, current on d-q plane, and current on z_1-z_2 plane.

three-phase induction machine compared with the conventional space vector PWM. However, as being compared with the control technique proposed in this paper, the sine-triangle PWM technique produces a larger amplitude of harmonic currents on the z_1-z_2 plane because the voltage vectors generated by the sine and the triangular carrier wave crossing cannot be guaranteed to have minimum projections on the z_1-z_2 plane.

From the comparison of the simulation results, it is apparent that much better control performance over previous approaches can be achieved by using the proposed technique.

V. Experimental Results

The dual three-phase induction machine drive system examined in this paper has been constructed to test the pro-

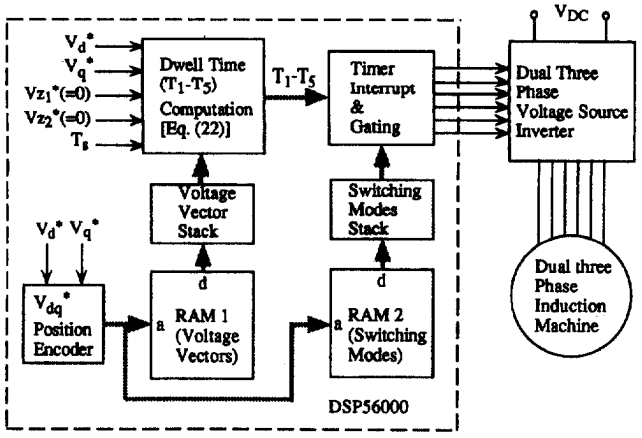

Fig. 8. Test system block diagram.

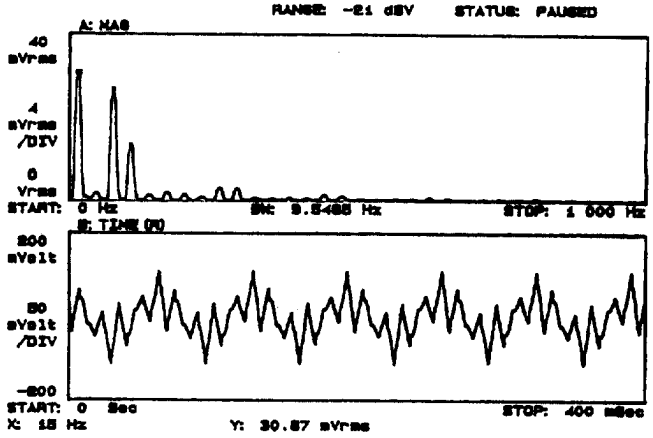

Fig. 9. Experimental results using the conventional space vector PWM. Upper trace: current spectrum; lower trace: machine phase current, 5 A (50 mv)/div.

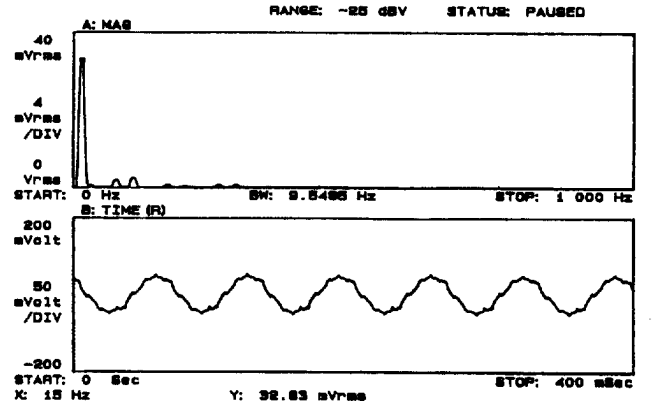

Fig. 10. Experimental results using the proposed space vector PWM. Upper trace: current spectrum; lower trace: machine phase current, 5 A (50 mv)/div.

posed analysis and control technique. The implementation uses IGBT's for the power switching devices and a MOTOROLA DSP56000 microprocessor for the controller. A five horsepower, four-pole induction machine with thirty-six stator slots was rewound to form a six-pole, dual three-phase machine for the test. The system block diagram is shown in Fig. 8, and the operating principle illustrated as follows.

The d-q plane is divided into 12 sections as indicated in Fig. 4, and the position of the voltage reference vector V_{dq}^* was coded accordingly and used as the addresses for RAM1 and RAM2. During each sampling period T_s, five out of thirteen switching modes were picked up from RAM2 and stored in the switching modes stack. Meanwhile, five voltage vectors corresponding to the five switching modes in the d-q-z_1-z_2 reference frame were picked up from RAM1 and stored in the voltage vector stack for the purpose of dwell time calculation. The dwell times for each of the five voltage vectors are calculated from (22) and used to control the timer interrupt interval. Gating signals are sent out in the timer interrupt subroutine and their widths are determined by the timer interrupt intervals.

To compare the performance of the proposed space vector PWM with the conventional method, both strategies were implemented in software. Sampling frequencies of 2 kHz for the proposed technique and 4 kHz for the conventional approach have been chosen to maintain the switching frequency for an individual IGBT in both cases to be equal at 2 kHz. Although this sampling frequency is far below the switching capability of an IGBT, the switching speed is limited by the instruction execution speed and the minimum achievable timer interrupt interval of the DSP. For the same reason, the machine for the tests was operated at 15 Hz rather than the rated 60 Hz.

The experimental results corresponding to the conventional space vector PWM are shown in Fig. 9. As expected, the harmonic currents on the z_1-z_2 plane, i.e., the 5th, 7th, 17th, and 19th, etc., are extraordinarily large due to the lack of control over currents on this plane. The performance of the proposed space vector PWM is illustrated in Fig. 10. Although the 5th and 7th harmonic currents are still appreciable due to the switching frequency limitation, very substantial reductions can be observed compared with the conventional method. The experimental results have sufficiently verified the correctness of the analysis and the feasibility of the proposed dual three phase induction machine control technique.

VI. Conclusion

This paper has presented a unified approach to space vector control of dual three-phase induction machines. While the machine examined specifically deals with the dual three-phase connection, it is clear that the approach may be readily extended to any machine having sinusoidally wound stator windings with any number of phases. It has often been stated that machines having a phase number greater than one are "all equivalent" from the modeling point of view. That is, it is said that all multi-phase machines effectively reduce to the same d-q-0 equivalent circuit model. This paper has demonstrated that this perception is false. In particular, even when the phase currents sum to zero, $m-3$ zero sequence and $6n \pm 1$ (n odd number) zero sequence components exist. It is further shown that careful attention to the control of these added zero sequence components are necessary to provide optimum current regulation of a multi-phase machine.

ACKNOWLEDGMENT

The authors are indebted to the member companies of WEMPEC for the facilities provided for the experimental test.

REFERENCES

[1] A. Nabae, I. Takahashi, and H. Akagi, "A new neutral-point-clamped PWM inverter," *IEEE Trans. Ind. Applicat.*, vol. IA-17, no. 5, pp. 518–523, Sept./Oct. 1981.

[2] T. M. Jahns, "Improved reliability in solid-state ac drives by means of multiple independent phase-drive units," *IEEE Trans. Ind. Applicat.*, vol. IA-16, no. 3, pp. 321–331, May/June 1980.

[3] J.-R. Fu and T. A. Lipo, "Disturbance free operation of a multiphase current regulated motor drive with an opened phase," *IEEE Trans. Ind. Applicat.*, vol. 30, no. 5, pp. 1267–1274, Sept./Oct. 1994.

[4] K. Gopakumar, V. T. Ranganathan, and S. R. Bhat, "Split-phase induction motor operation from PWM voltage source inverter," *IEEE Trans. Ind. Applicat.*, vol. 29, no. 5, pp. 927–932, Sept./Oct. 1993.

[5] M. A. Abbas, R. Christen, and T. M. Jahns, "Six-phase voltage source inverter driven induction motor," *IEEE Trans. Ind. Applicat.*, vol. IA-20, no. 5, pp. 1251–1259, Sept./Oct. 1984.

[6] E. E. Ward and H. Harer, "Preliminary investigation of an inverter fed 5-phase induction motor," *IEE Proc.*, June 1969, vol. 116(B), No. 6, pp. 980–984.

[7] C. L. Fortescue, "Method of symmetrical co-ordinates applied to the solution of polyphase networks," *AIEE Trans.*, vol. 37, pp. 1027–1115, 1918.

[8] D. White and H. Woodson, *Electromechanical Energy Conversion*. New York: Wiley, 1959.

[9] R. H. Nelson and P. C. Krause, "Induction machine analysis for arbitrary displacement between multiple winding sets," *IEEE Trans. Power App. and Syst.*, vol. PAS-93, pp. 841–848, May/June 1974.

[10] T. A. Lipo, "A d-q model for six phase induction machines," in *Int. Conf. Electric Machines*, Athens, Greece, Sept. 15–17, 1980, pp. 860–867.

[11] R. J. Schilling and H. Lee, *Engineering Analysis—A Vector Space Approach*. New York: Wiley, 1988.

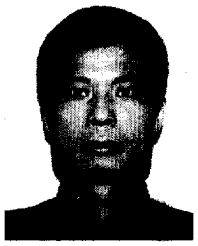

Yifan Zhao (S'91) received the B.S. degree from Jiaozuo College of Mining, P.R.C., in 1982, and the M.S. degree from the China University of Mining and Technology, in 1985, both in electrical engineering.

From 1985 to 1990, he was with the Industrial Automation Department, China University of Mining and Technology. He is currently a Ph.D. candidate at the Department of Electrical and Computer Engineering, University of Wisconsin, Madison. His research interests include the analysis, design, and control of electric machine drives, power electronics circuits, and microprocessor-based control systems.

Thomas A. Lipo (M'64–SM'71–F'87), for a photograph and biography, see p. 1078 of this issue.